Babeş-Bolyai University
Cluj-Napoca
Faculty of Physics
Biophysics Medical Physics
Specialization

MASTER'S DEGREE

Scientific Coordinator:

Prof.dr. Vasile Chiș

Graduate Student:

Diana-Gabriela Timaru

CLUJ-NAPOCA

2022

Babeş-Bolyai University
Cluj-Napoca
Faculty of Physics
Medical Physics Specialization

MASTER'S DEGREE

All-Atom Molecular Dynamics Investigations on the Interactions between D2 Subunit Dopamine Receptor and Three 11C-Labeled Radiopharmaceutical Ligands

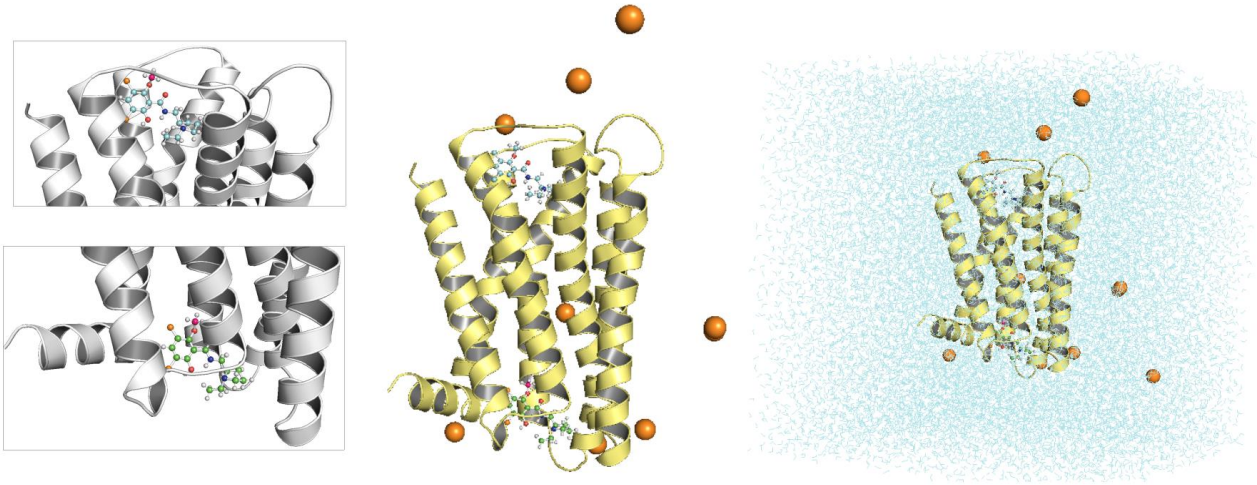

Scientific Coordinator:

Prof.dr. Vasile Chiş

Graduate Student:

Diana-Gabriela Timaru

CLUJ-NAPOCA

2022

Table of contents

ABSTRACT

It is well known that the dopamine neurotransmitter and its receptors play a crucial role in neuronal signal transfer and various metabolic processes. Using molecular dynamics (MD) approaches, the current work aims to identify and characterize the best binding poses between D2 dopamine receptor (D2DR) and three [^{11}C]-labeled synthetic compounds: [^{11}C]-FLB 457, raclopride ([^{11}C]-RACL), and halobenzazepine ([^{11}C]-SCH).

Previous studies have reported a high affinity of the FLB 457 compound for the D2 dopamine subunit. In addition, RACL is already being used as a PET scan radiotracer, tagged with [^{11}C]. On the other hand, while SCH 23290 has shown great specificity for the D1DR, it has been also demonstrated that this ligand antagonizes processes induced by other compounds with a direct effect on the D2 dopamine receptor.

In good agreement with experimental data, our research demonstrated that RACL ligand docked at the upper part of D2 dopamine receptor, has the highest interaction energy patterns.

Furthermore, these findings pave the way for future investigations. Perspectives consist of further MD studies with extensive production time and free energy calculations. The same set of ligands will be docked in the top pocket of the receptor, with the D2DR structure embedded in a DOPC/phospholipid bilayer membrane.

1. Introduction

Over the last decades, advances in computational technology have enabled the development of simulation approaches allowing a better characterization of a wide spectrum of biomolecular processes. The research of structural and dynamical properties at the atomic level is being used as a gateway to future experimental techniques employing conventional and quantum Molecular Dynamics (MD) simulations. MD simulations are useful methods for analyzing polymers and protein dynamics, predicting bulk characteristics, liquid states, and phase changes among other important applications [1].

Quantum mechanical calculations using density functional theory (DFT) or other real-space multi-grid approaches [2], shown to be reliable in predictive studies. However, there are a few drawbacks of biophysical simulations. Unfortunately, these approaches need a significant amount of resources and computer capacity. Although it is feasible to model a decent number of atoms across hundreds of picoseconds, such simulations are unquestionably impractical when it comes to complex biomolecular systems, which comprise thousands of atoms with relevant time frames ranging from nanoseconds to seconds. As a result, traditional MD approaches are best suited for simulating large biomolecular systems [2].

The purpose of the present research is to identify the binding positions in which the D2 dopamine receptor (D2DR) would most likely interact with three [^{11}C]-labeled synthetic compounds widely used for medical imaging investigations, such as PET/CT or PET/MRI scans, and to characterize the structural and dynamical behavior of the preformed interacting complexes. The compounds of interest related to this thesis are: raclopride (RACL) [3-5], halobenzazepine (SCH 23390) [6] and FLB 457 [7-10].

1.1. Structures of Interest

1.1.1. D2 Dopamine Receptor

The dopamine neurotransmitter and its receptors are known to play an important role in neuronal signal transductions, regulating specific processes such as reward, addiction, coordinated movement, metabolism, and hormone secretion [11, 12]. Schizophrenia, Parkinson's disease, attention deficit hyperactivity disorder, depression, nausea, and vomiting are all manifestations of negative outcomes produced by dopaminergic system dysregulation. Dopamine's behavior is mediated by a group of five G-protein coupled receptors [13].

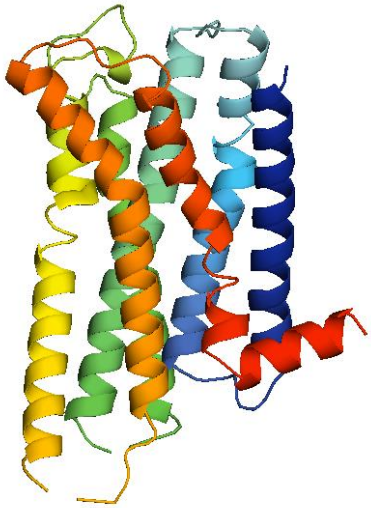

Figure 1.1. *- D2DR structure manipulated in PyMol viewing program [14]*

The D2DR (Fig. 1.1) is the primary target for antipsychotic medications, both typical and atypical, as well as those used to treat Parkinson's disease. D2DR functions as an auto receptor and is crucial in controlling dopamine release. However, most D2DR-targeting medications may cause major brain damages that might involve life-threatening effects including abnormal movement control and severe cognitive symptoms. Thus, investigating and comprehending the D2DR's structure at the molecular level becomes essential for improved medication development.

Previous prediction investigations [11] resulted in the finding of key bonding sites in the human D2DR. However, only one binding site was shown to be suitable for bonding with the other agonists studied such as: domperidone, spiperone, apomorphine etc. [11]. The predicted site of dopamine is found within the top third of the 7-TM involving 3-6 TM domains. Other examples of important dopamine binding sites of D2 receptors in humans (Fig. 1.2) are:

• **Asp-114** found in TM3. The bridge occurs between the carboxyl group of aspartate and the main amino group of dopamine.

- **Ser-193** and **Ser-197** in **TM5.** Both residues bind to dopamine catechol ring's metahydroxyd (2.7 Å) and parahydroxyd (2.7 Å) groups through H-bonds, which play an essential role in dopamine recognition. **Ser-197** has also been found in all five of the human dopamine receptors.

- **Phe-110, Met-117, Cys-118 (TM3), Phe-164 (TM4), Phe-189, Val-190 (TM5), Trp-386, Phe-390** and **His-394 (TM6)** assemble a predominantly hydrophobic pocket for dopamine.

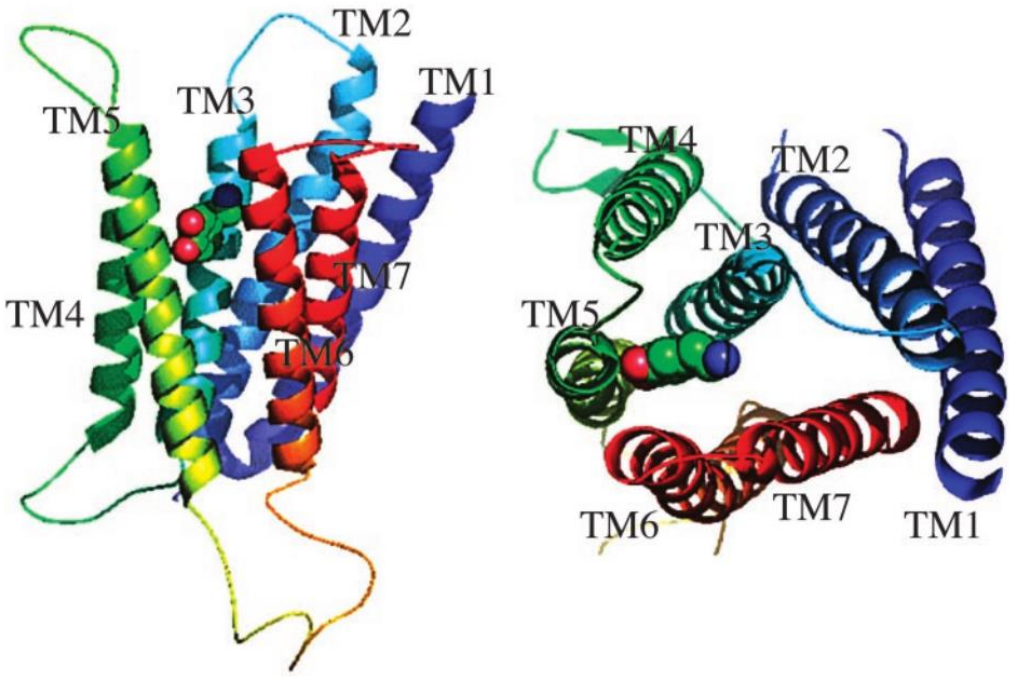

Figure 1.2 - Predicted binding sites of dopamine (shown in spheres) in the structure of human dopamine D2 receptor [11].

1.1.2. FLB 457

FLB 457 is a synthetic molecule with a high affinity for the D2 dopamine receptor in vitro (K_i=18 pmole). [7-9] Moreover, the compound (Fig. 1.3) presented high affinities for D2 (K_i=0.022 nM in rat striatum tissue, $^{[125]}$NCQ 298 radioligand) and D3 (K_i=0.017 nM in cell membranes tissue, $^{[125]}$NCQ 298 radioligand) dopamine receptors, however lower binding affinities were observed to other putative central receptors in high concentrations [10].

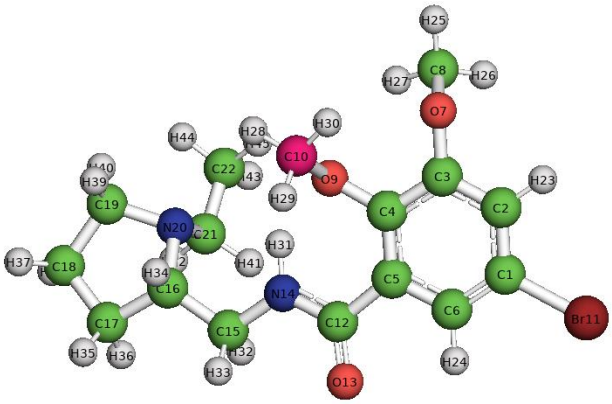

Figure 1.4. - *FLB structure (in pink, the ^{11}C labeled atom)*

1.1.3. Halobenzazepine

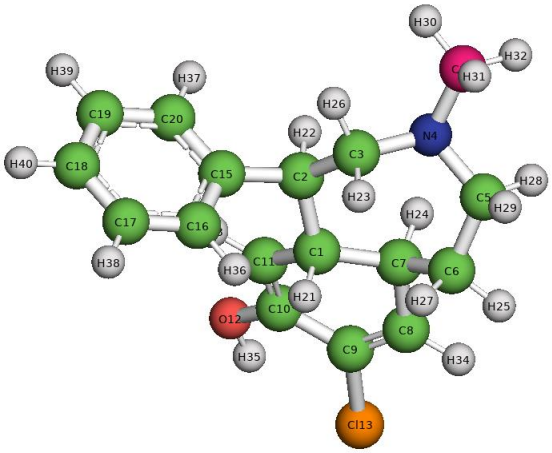

Figure 1.4. - *SCH structure (in pink, the ^{11}C labeled atom)*

The synthetic compound halobenzazepine (Fig. 1.4), also known as SCH 23290 (7-chloro-3-methyl-1-phenyl-1,2,4,5-tetrahydro-3-benzazepin-8-ol), has little impact on D2-type of dopamine receptors.. On the other hand, it serves as an antagonist for the D1DR. An experiment [6] conducted on rats found that SCH reduces the mortality rate from dextroamphetamine overdose as well as cocaine overdose (although just the minimal dosage was used in this instance), but had little to no impact on methamphetamine overdose. The compound's chemical formula is $C_{17}H_{18}CINO$, and its molar mass is 287.78 g/mol.

1.1.4. Raclopride

Raclopride (3,5-dichloro-N-[(2S)-1-ethylpyrrolidin-2-yl]methyl)-2-hydroxy-6-methoxybenzamide is another synthetic molecule that serves as a selective D2DR antagonist (K_i=18 nM) [3]. It is most frequently used PET radiotracer for assessing DA variations in synaptic dopamine rates but can be also used to diagnose movement impairments and to keep Huntington's disease under control [4, 15]. Another use of RACL is to assess the potency and neurotoxicity of dopaminergic medications. RACL has the chemical formula $C_{15}H_{20}Cl_2N_2O_3$ and a molar mass of 347.236 g/mol [5].

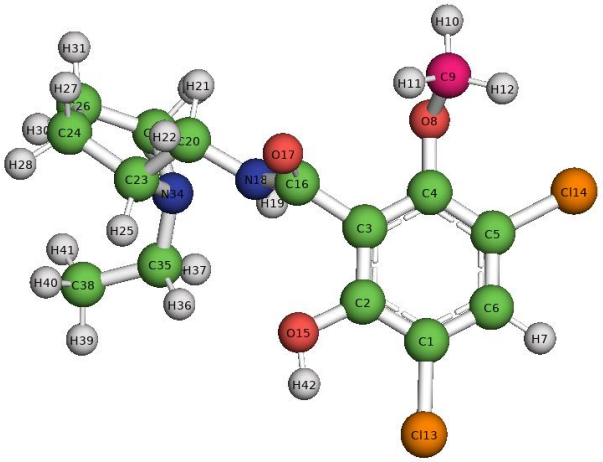

Figure 1.5. - *RACL structure (in pink, the ^{11}C labeled atom)*

1.2. Molecular Dynamics Simulations

The primary goal of MD methods is to replicate what atoms behave like in real life. A discretization of Newton's equations of motion is essential in classical MD simulations for computing the trajectories of a set of interacting atoms. Atom-to-atom interactions generate forces. These forces are often defined in terms of interatomic empirical potentials, which are responsible for the bonding between atoms [1, 16]. It is possible to define how atoms interact with one another using a specific potential energy function. Given the locations of nearby atoms, the energy function calculates the force experienced by each atom. Applying the Newton's equations of motion helps to analyze how forces impact the movements of atoms and, as a result, anticipates the dynamical behavior of the system [17]. The characterization of the interaction between particles is possible using the following components: the potential functions that describe the

potential energy, the forces obtained from the derivation of the potential energies and the parameters employed in these potential functions.

1.2.1. Non-bonded interactions

Non-bonded potential functions are being described by: Lennard-Jones or Buckingham potentials, and Coulomb or modified Coulomb potential. Non-bonded interactions are pair-additive:

$$V(\mathbf{r}_1, \ldots \mathbf{r}_N) = \sum_{i<j} V_{ij}(\mathbf{r}_{ij}); \tag{1.1}$$

$$\mathbf{F}_i = -\sum_j \frac{dV_{ij}(r_{ij})}{dr_{ij}} \frac{\mathbf{r}_{ij}}{r_{ij}} \tag{1.2}$$

Due to the fact that the potential depends on the scalar distance, interactions are centro-symmetric. For example, the partial force on *i* particle has the opposite direction of the partial force on particle *j* (Fig. 1.6). The non-bonded interactions consist of a repulsion term, a dispersion term and a Coulomb term. Both the repulsion and the dispersion terms are combined in either the Lennard-Jones or in the Buckingham potential. Moreover, charged atoms act through the Coulomb term [18].

1.2.1.1. Lennard-Jones

The Lennard-Jones potential V_{LJ}between two atoms is given by [18]:

$$V_{LJ}(r_{ij}) = \frac{C_{ij}^{(12)}}{{r_{ij}}^{12}} - \frac{C_{ij}^{(6)}}{{r_{ij}}^{6}} \tag{1.3}$$

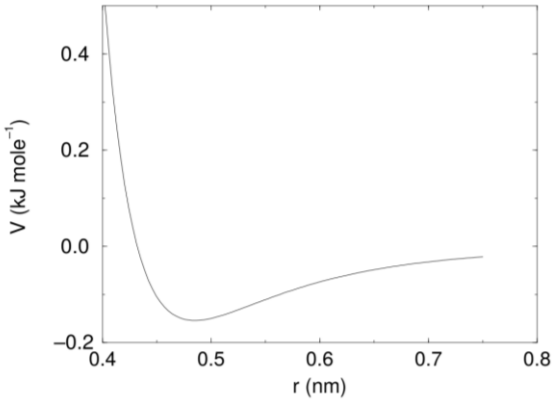

Figure 1.6 *-The Lennard-Jones potential [18].*

The $C_{ij}^{(12)}$ and $C_{ij}^{(6)}$ parameters depend on the atom type pairs and as a result, these parameters are selected from a matrix of Lennard-Jones parameters [18]. The derived form of the LJ potential has as a result the form of the force:

$$\mathbf{F}_i(\mathbf{r}_{ij}) = \left(12 \frac{C_{ij}^{(12)}}{{r_{ij}}^{13}} - 6 \frac{C_{ij}^{(6)}}{{r_{ij}}^{7}} \right) \frac{\mathbf{r}_{ij}}{r_{ij}} \tag{1.4}$$

1.2.1.2. Coulomb interactions

The Coulomb interaction between two charged particles is obtained from the following equation:

$$V_c(r_{ij}) = f \frac{q_i q_j}{\varepsilon_r r_{ij}} \tag{1.5}$$

where $f = \frac{1}{(4\pi\varepsilon_0)} = 138.935458$[18] .

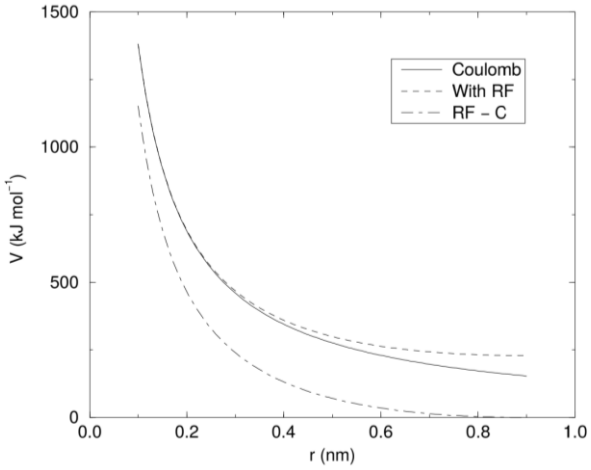

Figure 1.8. *-The Coulomb interaction (for particles with equal signed charge) with and without reaction field. The dot-dashed line is the same as the dashed line, except for a constant [18].*

As a result, the force is:

$$\mathbf{F}_i(\mathbf{r}_{ij}) = f\frac{q_i q_j}{\varepsilon_r {r_{ij}}^2}\frac{\mathbf{r}_{ij}}{r_{ij}} \tag{1.6}$$

If a constant dielectric environment beyond the cut-off $r_c$is considered, with a dielectric constant of ε_{rf}, it is possible to change the Coulomb interaction for homogeneous systems [18]. Therefore, the potential takes the following form:

$$V_{crf} = f\frac{q_i q_j}{\varepsilon_r r_{ij}}\left[1+\frac{\varepsilon_{rf}-\varepsilon_r}{2\varepsilon_{rf}+\varepsilon_r}\frac{{r_{ij}}^3}{r_c^3}\right] - f\frac{q_i q_j}{\varepsilon_r r_c}\frac{3\varepsilon_{rf}}{2\varepsilon_{rf}+\varepsilon_r} \tag{1.7}$$

At the $r_c$cut-off, the constant right member of the equation has as a result a potential equaling zero. For charged cut-off spheres, this correlate to a neutralization with homogeneous background charge [18]. To simplify the derivation for obtaining the form of the force a few notations can be made:

$$V_{crf} = f\frac{q_i q_j}{\varepsilon_r}\left[\frac{1}{r_{ij}} + k_{rf}\, {r_{ij}}^2 - c_{rf}\right] \tag{1.8}$$

$$k_{rf} = \frac{1}{r_c^3}\frac{\varepsilon_{rf} - \varepsilon_r}{(2\varepsilon_{rf} + \varepsilon_r)} \tag{1.9}$$

$$c_{rf} = \frac{1}{r_c} + k_{rf}\, r_c^2 = \frac{1}{r_c}\frac{3\varepsilon_{rf}}{(2\varepsilon_{rf} + \varepsilon_r)} \tag{1.10}$$

Following these steps, the force can be written as follows:

$$\mathbf{F}_i(\mathbf{r}_{ij}) = f\frac{q_i q_j}{\varepsilon_r}\left[\frac{1}{{r_{ij}}^2} - 2k_{rf} r_{ij}\right]\frac{\mathbf{r}_{ij}}{r_{ij}} \tag{1.11}$$

1.2.2. Bonded interactions

Bonded interactions are based on a fixed list of atoms. These are not solely pair interactions. However, they include 3- and 4-body interactions as well. There are a few types of interactions: *bond stretching (2-body), bond angle (3-body), dihedral angle (4-body)* and *improper dihedral interaction,* used to force atoms to stay in the same plane or to avoid the construction of a mirror image [18].

1.2.2.1 Harmonic potential

The bond stretching between two covalently bonded atoms *i* and *j* is described by a harmonic potential of the following form [18]:

$$V_b\,(r_{ij}) = \frac{1}{2}k_{ij}^b(r_{ij} - b_{ij})^2 \tag{1.12}$$

Consequently, the force is:

$$\mathbf{F}_i(\mathbf{r}_{ij}) = k_{ij}^b(r_{ij} - b_{ij})\frac{\mathbf{r}_{ij}}{r_{ij}} \tag{1.13}$$

1.2.2.2 Morse potential bond stretching

The Morse potential is used for systems that need an anharmonic bond stretching potential. The potential well is asymmetrical and the force is zero at infinite distance. [18] The functional form is:

$$V_{morse}(r_{ij}) = D_{ij}[1 - \exp(-\beta_{ij}(r_{ij} - b_{ij}))]^2, \tag{1.14}$$

and by derivation we get the corresponding force:

$$\begin{aligned}\mathbf{F}_{morse}(\mathbf{r}_{ij}) &= 2D_{ij}\beta_{ij}\exp(-\beta_{ij}(r_{ij} - b_{ij}))* \\ &\quad [1 - \exp(-\beta_{ij}(r_{ij} - b_{ij}))]\frac{\mathbf{r}_{ij}}{r_{ij}},\end{aligned} \tag{1.15}$$

with the following parameter:

$$\beta_{ij} = \sqrt{\frac{k_{ij}}{2D_{ij}}} \tag{1.16}$$

Knowing that (r_{ij}-b_{ij}) can be approximated using Taylor expansion, we will get the final result as follows:

$$\begin{aligned} V_{morse}(r_{ij}) &= D_{ij}[1-\exp(-\beta_{ij}(r_{ij}-b_{ij}))]^2 \\ &= D_{ij}[1-(1-\sqrt{\tfrac{k_{ij}}{2D_{ij}}}(r_{ij}-b_{ij}))]^2 \\ &= \tfrac{1}{2}k_{ij}(r_{ij}-b_{ij}))^2 \end{aligned} \tag{1.17}$$

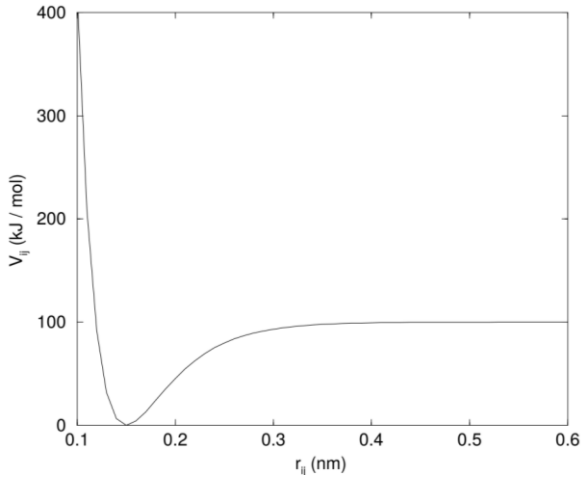

Figure 1.9 -*The Morse potential with bond length 0.15 nm [18].*

1.2.2.3 Urey-Bradley potential

The Urey-Bradley bond-angle vibration is given by the harmonic potential on angle Θ_{ijk} and a harmonic correction term on the distance between the atoms *i* and *k*. The energy is given by the following equation [18]:

$$V_a(\theta_{ijk}) = \frac{1}{2}k^{\theta}_{ijk}(\theta_{ijk}-{\theta_{ijk}}^0)^2 + \frac{1}{2}k^{UB}_{ijk}(r_{ik}-r^0_{ik})^2 \tag{1.18}$$

1.2.2.4 Bond-bond cross term

For three given particles *i-j-k* forming the bonds *i-j* and *k-j*, the bond-bond cross term is given by [18]:

$$V_{rr'} = k_{rr'} \left(|\mathbf{r}_i - \mathbf{r}_j| - r_{1e}\right) \left(|\mathbf{r}_k - \mathbf{r}_j| - r_{2e}\right) \tag{1.19}$$

where k_{rr} is the force constant and r_{1e} and r_{2e} are the equilibrium bond lengths. The force has the following form for the *i*-particle:

$$\mathbf{F}_i = -k_{rr'} \left(|\mathbf{r}_k - \mathbf{r}_j| - r_{2e}\right) \frac{\mathbf{r}_i - \mathbf{r}_j}{|\mathbf{r}_i - \mathbf{r}_j|} \tag{1.20}$$

By swapping *i* and *k,* it is possible to calculate the force for *k*, and from: F_j=-F_i-F_k, we may determine the force for particle *j* [18].

1.2.2.5 Bond-angle cross term

Cross terms represent the terms containing atoms from both quantum mechanics (QM) and molecular mechanics (MM) regions at the same time, consisting of bonded and non-bonded interactions. The bonded interactions are taken from the force field used to describe the MM region, while the non-bonded interactions are separated into van der Waals and electrostatic contributions [18].

The bond-angle cross term for particles *i , j, k* is given by:

$$V_{r\theta} = k_{r\theta}\left(|\mathbf{r}_i - \mathbf{r}_k| - r_{3e}\right)\left(|\mathbf{r}_i - \mathbf{r}_j| - r_{1e} + |\mathbf{r}_k - \mathbf{r}_j| - r_{2e}\right) \quad (1.21)$$

and the force is:

$$\mathbf{F}_i = -k_{r\theta}\left[\left(|\mathbf{r}_i - \mathbf{r}_k| - r_{3e}\right)\frac{\mathbf{r}_i - \mathbf{r}_j}{|\mathbf{r}_i - \mathbf{r}_j|} + \left(|\mathbf{r}_i - \mathbf{r}_j| - r_{1e} + |\mathbf{r}_k - \mathbf{r}_j| - r_{2e}\right)\frac{\mathbf{r}_i - \mathbf{r}_k}{|\mathbf{r}_i - \mathbf{r}_k|}\right] \quad (1.22)$$

1.2.2.6 Improper dihedrals

The role of the improper dihedrals is to maintain the planar characteristic of a planar group (e.g. aromatic rings). Also they prevent molecules from flipping over to their mirror images. The simplest improper dihedral potential is a harmonic potential [18]:

$$V_{id}(\xi_{ijkl}) = \frac{1}{2}k_\xi(\xi_{ijkl} - \xi_0)^2 \quad (1.23)$$

1.2.3. Force fields

A force field (FF) is used to describe the dependence of the energy of a system on the coordinates of its particles [19]. This description is based on a mathematical expression and up to present, several force-fields have been developed with considerable coverage of drug-like molecules [19].

Force fields are composed by an analytical form of the interatomic potential energy and a set of parameters that are usually obtained from two methods. First method is the *ab initio* or

semi-empirical quantum mechanical calculations. The latter one is to fit experimental data such as NMR, X-ray and electron diffraction, infrared, Raman and neutron spectroscopy etc. As a mean of exemplification, molecules can be seen as a set of atoms held together by harmonic forces. Using a simplified model that is valid in a stimulated region, FFs replace the potential. As simple as the things are presented however, FFs are able to describe and reproduce the most important properties of a system [20]. A typical FF expression is presented below:

$$U = \sum_{\text{bonds}} \frac{1}{2} k_b (r - r_0)^2 + \sum_{\text{angles}} \frac{1}{2} k_a (\theta - \theta_0)^2 + \sum_{\text{torsions}} \frac{V_n}{2} [1 + \cos(n\phi - \delta)] + \sum_{\text{improper}} V_{imp} + \sum_{\text{LJ}} 4\epsilon_{ij} \left(\frac{\sigma_{ij}^{12}}{r_{ij}^{12}} - \frac{\sigma_{ij}^{6}}{r_{ij}^{6}} \right) + \sum_{\text{elec}} \frac{q_i q_j}{r_{ij}}, \quad (1.24)$$

where the first four terms describe intramolecular or local contributions to the total energy, respectively to: bond stretching, angle bending, dihedral and improper torsions. The last two terms refer to the repulsive and Van der Waals interactions, as well as Coulombic interactions [20].

1.2.4. Periodic Boundary Conditions

Periodic boundary conditions (PBC) are used in molecular dynamics simulation to prevent issues with boundary effects, usually the result of finite sizes. The PBC converts the system into an infinite one and that leads to periodicity effects [18].

A very important aspect that must be taken into account is that if a given molecule "leaves" the box on one side and enters through its opposite side, due to the fact that molecules are supposed to diffuse, the periodicity effect is no longer considered as an abnormal conduct [18].

1.2.5. System Equilibration

A thermodynamic system's macroscopic state can be described by state variables: particle number, volume, temperature, pressure, total energy. The connection between these variables are the equations of state [21]. For MD simulations some state variables must be calculated, whereas others represent the external parameters. A short representation of these variables can be seen in Table 1.1.

Table 1.1. *Table of ensembles of a thermodynamic system*

Ensemble	Observable parameters	Constant parameters	Observations
Microcanonical Ensemble (NVE)	-particle number N; -Volume V; -total energy E.	-temperature T; -pressure P.	Modifying molecular dynamics that change E and V, to keep T and P constant.
Canonical Ensemble (NVT)	-particle number N; -volume V; -temperature T.	-total energy E; -pressure P.	Thermostat-an algorithm that adds and removes energy in order to obtain constant temperature.
Isothermal-isobaric Ensemble (NPT)	-particle number N; -pressure P; -temperature T.	-total energy E; -volume V.	Barostat- an algorithm that changes the volume in order to obtain constant pressure.

Any change brings the system out of the equilibrium state. To reach the equilibrium state again, a number of time steps is required in order to be able to measure the observables.

1.2.6. Simulation Flow Chart

The flow chart represents the steps needed to be considered in order to be able to have a successful MD simulation. There is no typical flow chart because the systems depend on each scientist's interests, but a common flowchart is illustrated in Figure 1.11. However, when it comes to simulating a protein-ligand complex, even though it is similar, there are a few differences due to the fact that the ligand of interest is a non-proteic structure.

Such structures are not automatically recognized by the FFs (are seen as unknown species) and therefore, before generating the topology of the ligand, external force fields (e.g. CGenFF server) are used to process and return the parameters compatible with the FF used in that simulation.

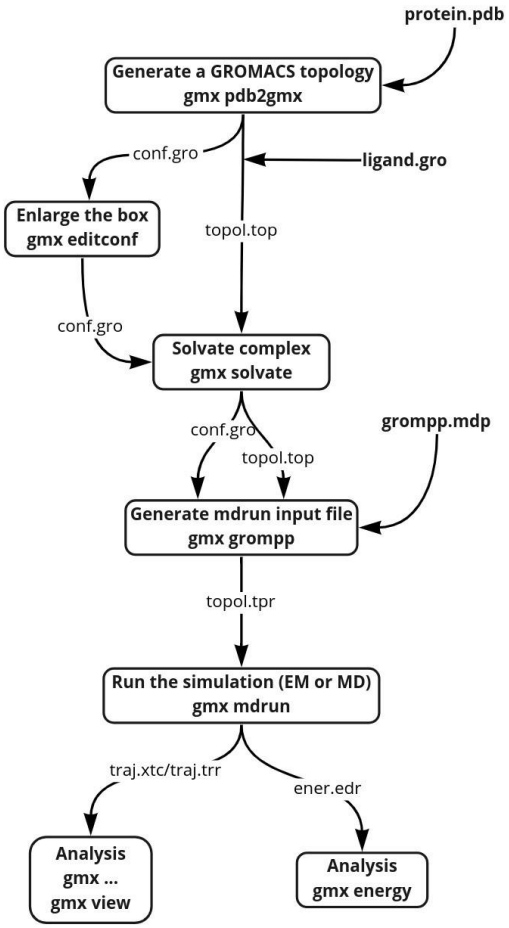

Figure 1.11. - *Flow Chart*

2. Methodology

The coordinates of the receptor (D2 subunit) were obtained from the Protein Data Bank (PDB Code: 6CM4) database [12]. A dock-prep of the receptor and ligands was examined using the PyMOL [14] visualization tool and the UCSF Chimera [22] software. For the molecular docking partial charges and hydrogen atoms were inserted. The GROningen MAchine for Chemical Simulations (GROMACS) software [23] was used to construct the topology files for all of the complexes (receptor and ligands). For ions, water molecules, and D2 receptor characteristics, the CHARMM36 force field [19] was employed. The CGenFF (CHARMM General Force Field) server was used to generate the ligands' parameters [19].

A molecular docking technique was used to establish the best binding poses of the ligands against D2DR [24, 25]. The docking computations were performed on the Swiss Dock server [26], and the resulting clusters were ranked based on their full-fitness (FF) score function and Gibbs free energies. The findings indicated that all ligands presented two preferred docking sites (with higher FF absolute values) at the receptor level (top and bottom pockets), from where a total of six docked positions were selected for further investigations.

The docked receptor–ligand complexes were subsequently solvated using a TIP3P water model [27]. The solvated and neutralized (with counter ions) systems were afterwards minimized in 50,000 steps using the steepest descent algorithm, to eliminate any possible steric clashes.

The receptor–ligand complexes were then equilibrated for 10 ns in an NVT ensemble with a modified Berendsen thermostat set to 310 K [28]. With a time constant of 0.1 ps, temperature coupling was attributed to two different groups (D2DR-ligand and water-ions). The last frame of the NVT ensemble was utilized for the 10 ns NPT equilibration in isotropic pressure coupling type with a time constant of 1.0 ps and 1 bar pressure. During both the NVT and NPT ensembles, all ligands have been restrained. Our D2DR+RACL system is illustrated in Figure 2.1.

H-bond holonomically constraints were used using the LINCS algorithm [29], and Particle mesh Ewald (PME) [29] calculation method was employed for long-range electrostatic description. A cut-off distance of 12 Å was used for van der Waals and short-range electrostatic potentials .

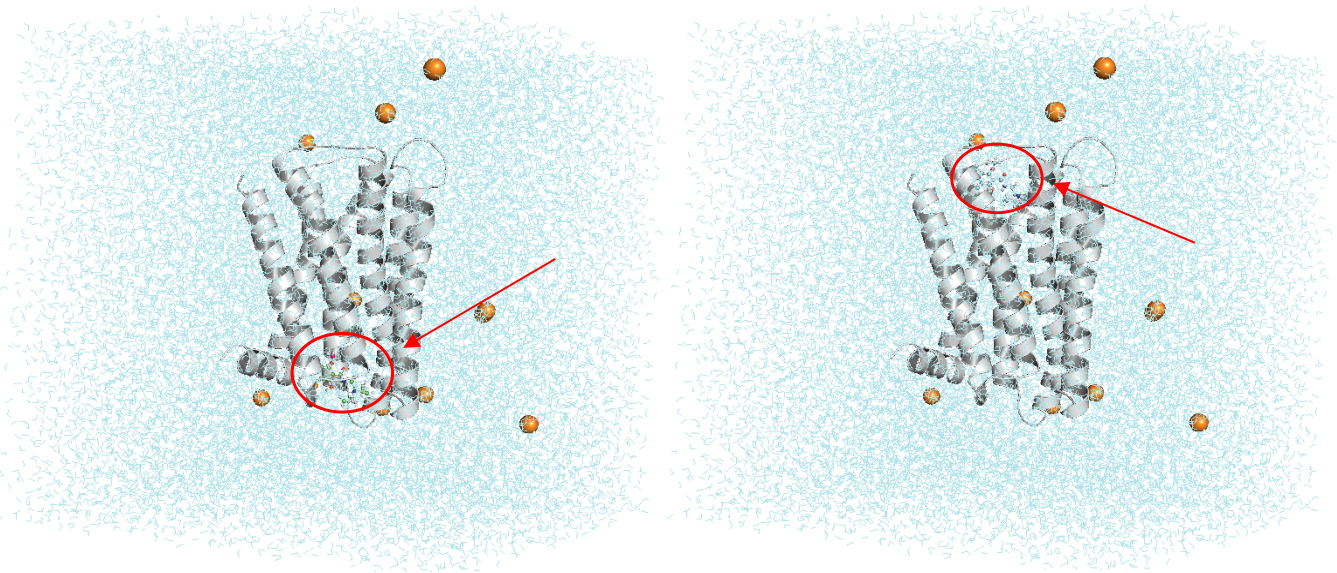

Figure 2.1. *- NPT ensemble at 310K and 1 bar of D2DR-LIG system docked at the bottom (left) and at the top (right)*

Multiple MD run productions with PBC for 50 ns with a time step of 2 fs were conducted in the NPT ensemble without restraints.

3. Results and Discussions

3.1. Docking Analysis

A total of 48 clusters for FLB, 43 clusters for RACL, and 33 clusters for SCH were obtained using the blind docking technique for the ligand binding modes at the top of the receptor (Table 3.1). The FLB ligand resulted in 28 docked clusters for the same site, RACL had 19 docked positions, and for SCH, 21 clusters of possible interest were found. The resulted clusters docked at the exterior sections of D2DR had lower docking scores (and substantially lower ΔG absolute values) and therefore were not considered for further investigations [30].

Table 3.1. *- Molecular docking results for D2DR-ligand top complexes [30].*

FLB		RACL		SCH	
Full-Fitness Score	ΔG (kcal/mol)	Full-Fitness Score	ΔG (kcal/mol)	Full-Fitness Score	ΔG (kcal/mol)
−1168.39	−7.954	−1171.87	−7.616	−1134.33	−7.126

We evaluated a special grid search strategy for the bottom portion of the receptor (Table 3.2), characterized by the following parameters: the center of the box was set at 45 x 44 x 69 Å, with 68 points in the x-dimension, 66 points in the y-dimension, and 50 points in the z-dimension. From a total of 45 clusters for the FLB ligand, 31 were docked within D2DRs. For the RACL ligand, 27 out of 42 clusters were docked inside D2DRs. However, only 13 docked clusters were found for the SCH ligand at D2DR's bottom position, the smallest number among all ligands [30].

Table 3.2. *- Molecular docking results for D2DR-ligand bottom complexes [30].*

FLB		RACL		SCH	
Full-Fitness Score	ΔG (kcal/mol)	Full-Fitness Score	ΔG (kcal/mol)	Full-Fitness Score	ΔG (kcal/mol)
−1157.05	−7.44	−1156.43	−6.899	−1103.53	−4.929

3.2. Solvent Accessible Surface Area

The hydrophilic and hydrophobic profiles (Figure 3.1) show lower values for ligands docked at the top region of the receptor, when compared to the bottom docked position where all ligands remained inside the D2DR docked position. The FLB ligand docked at the bottom part of the receptor presented the highest SASA average value of 5.63 nm^2 [30].

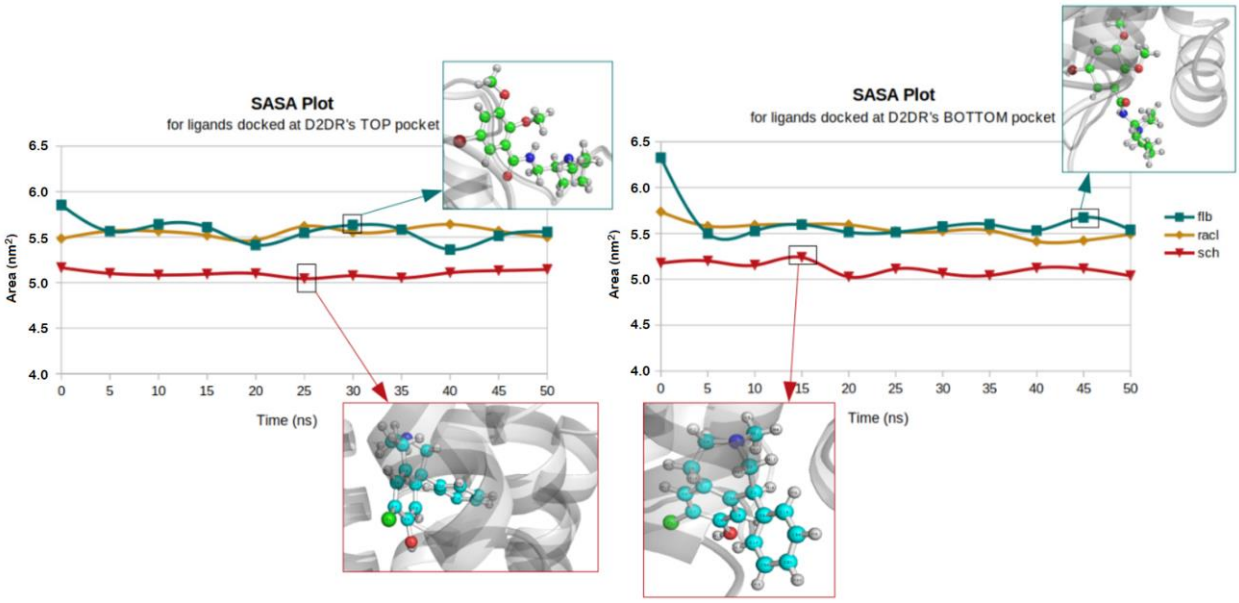

Figure 3.1. *- SASA profiles for ligands docked at D2DR's top (left) and bottom (right) positions [30].*

Due to D2DR's secondary structural components at its bottom section, where random coils and turns are more common, the aliphatic chain of the FLB ligand showed higher dynamic fluctuation rates. The greatest SASA value for the same ligand and docked position was 6.32 nm^2 [30].

The SCH ligand, docked at the top of D2DR, had the maximum retention from solvent exposure, with an average value of 5.10 nm^2. However, for the same ligand but in the opposite docked position, we observed a spontaneous behavior at around 15 ns when the SCH aromatic C6

ring became highly exposed to solvent molecules. In contrast, the RACL ligand displayed a stable behavior across the two D2DR docked sites with identical SASA values. The average SASA value for RACL situated at D2DR's top pocket was 5.55 nm^2, whereas its SASA value for D2DR bottom docked position was 5.54 nm^2 [30].

Another factor to consider for ligand solvent accessibility profiles is their molecular geometry. The ligand with a shorter chain and, as a result, fewer atoms (SCH has 38 atoms) had lower solvent exposure profiles at both receptor extremities [30].

RACL (42 atoms) and FLB (45 atoms) were more prone to hydrophilic behavior because their aliphatic chains were longer and more likely to interact with solvent molecules (FLB > RACL > SCH). Except from the previously indicated circumstance (associated to SCH), the phenyl groups (cyclic C_6H_5 - groups) of all three ligands retained their hydrophobic chemical patterns during the entire MD productions of 50 ns [30].

3.3. Radius of Gyration

Since the secondary structure analysis of D2DR revealed no significant differences and the alpha-helical content was the most prevalent structural component, the receptor's gyration profiles were not considered in this study. The analysis of the compactness profiles revealed that the gyration patterns between the top and bottom D2DR docked positions are similar, indicating that there are no substantial structural changes of the ligands (Figure 3.2). The FLB ligand presented the highest gyration radius of 0.41 nm for both D2DR docked pockets [30].

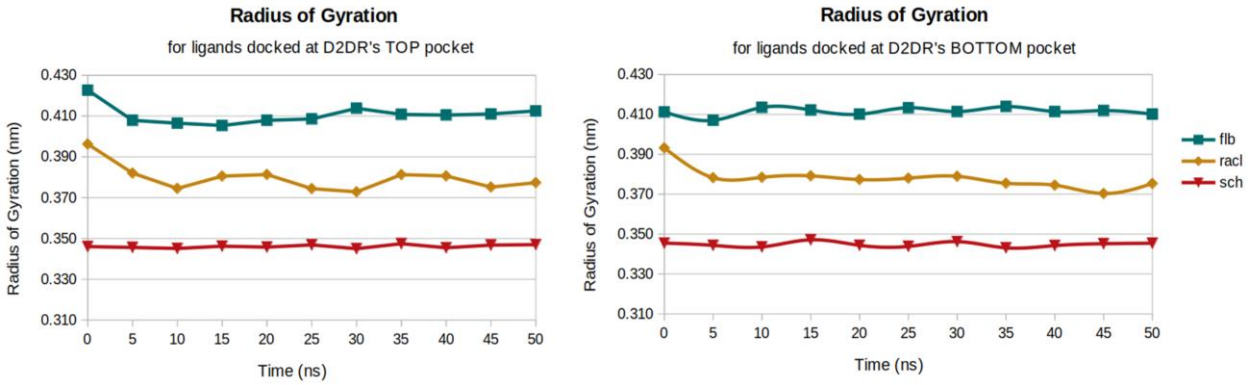

***Figure 3.2**. - Radius of gyration profiles for the two sets of ligands [30].*

The SCH ligand docked on both D2DR interaction sites had the lowest Rg average value of 0.34 nm. On the other hand, RACL ligand docked on both D2DR pockets had greater fluctuations in the ligands' compactness profiles over the MD simulations. These variations occurred during the first 10 ns of simulation time and concluded in a gyration average value of 0.38 nm [30].

3.4. Root-Mean-Square Fluctuations

The RMSF data show that the RACL ligand from the bottom part of the receptor has the highest atomic fluctuations with an average RMSF value of 0.15 nm, while the SCH ligand has the lowest fluctuation rate with an average RMSF value of 0.06 nm. The FLB and RACL ligands presented the same average RMSF value of 0.12 nm for the top docked pocket of D2DR [30].

The lower gyration values of 0.34 nm and the lower SASA values for both D2DR docked sites are consistent with the lower fluctuations of the SCH ligand (Figure 3.3). Similarly, when its gyration profiles are studied, a good correlation between RACL's enhanced flexibility and its gyration behavior was detected [30].

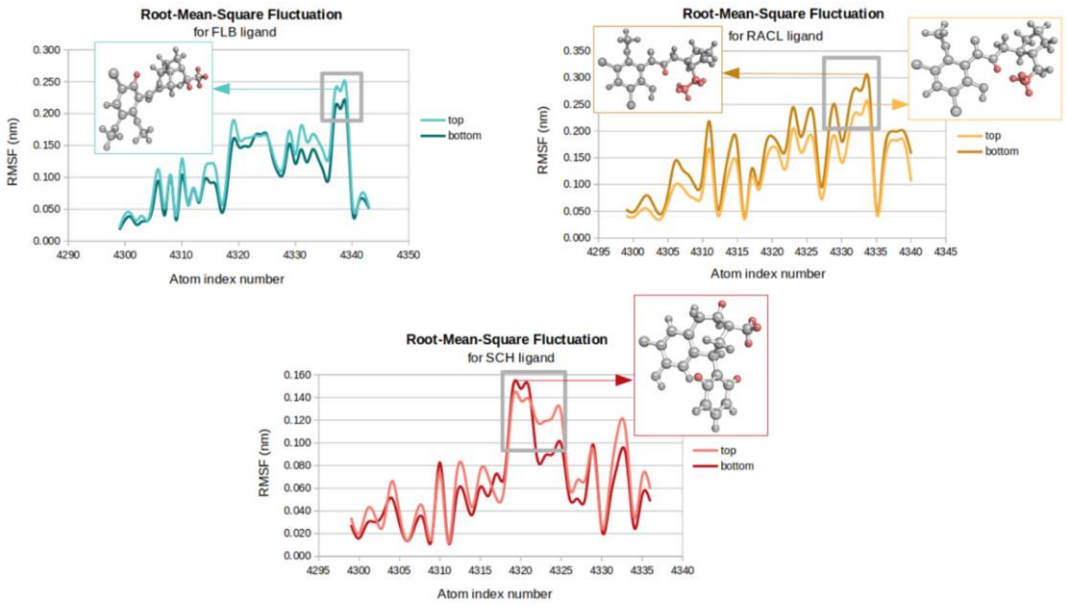

Figure 3.3. *- RMSF plots of D2DR's docked ligands [30].*

The lowest average values for the SCH ligand docked on both D2DR extremities were associated with the high fluctuations of six H atoms, of which three were engaged in the decreased number of degrees of freedom relating to the ligand's short aliphatic chain [30].

In contrast, the higher fluctuation rates observed for the RACL and FLB ligands located at the bottom of the D2DR are characterized by strong fluctuations of the CH_3-CH_2- atoms from their straight-chain alkyl groups, whereas for the same ligands docked at the top of the receptor the most prevalent motions corresponded to the methyl (CH_3-) groups from their aliphatic terminal chain [30].

The RMSF results are in good agreement with SASA profiles and gyration behavior of all ligands. Due to higher atomic fluctuations of the RACL and FLB ligands, the solvent exposure regions on both D2DR docked positions were also higher , therefore resulting in significant increases of the gyration values [30].

3.5. Root-Mean-Square Deviations

The ligands docked at the top position of the D2DR exhibit comparable fluctuation rates to those docked at the bottom part of the receptor. The most unstable molecule was the FLB ligand located on both D2DR pockets, with average RMSD values of 0.20 nm for the upper docked position and 0.19 nm for the lower one . Another significant RMSD value of 0.18 nm was detected for the RACL ligand located at the bottom part of D2DR [30].

Taking into account the variations between ligands bound at the superior and inferior part of the receptor, the SCH ligand presented the lowest RMSD value of 0.09 nm for both D2DR positions. Nonetheless, for the RACL ligand the RMSD profile (Figure 3.4) reveals higher atomic deviations for the D2DR's bottom part (0.18 nm), when compared to the top D2DR docked position (0.14 nm) [30].

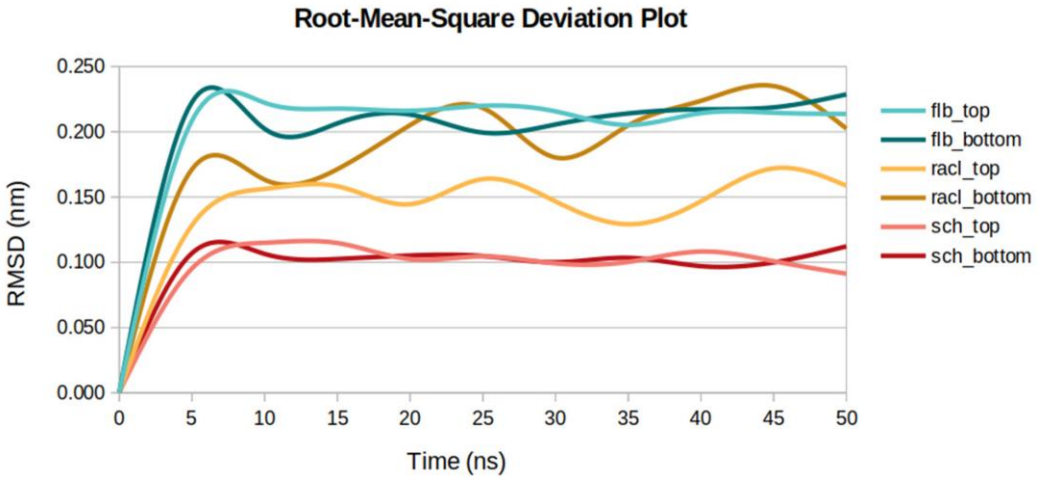

Figure 3.4. *- RMSD values for the three ligands docked at the top and bottom parts of D2DR [30].*

Additionally, the RMSD profiles for the SCH molecule (of 0.09 nm) docked on both parts of the receptor are in good agreement with the ligand's Rg minimum value of 0.34 nm and its lowest RMSF of 0.07 nm for the top D2DR docking site and 0.06 nm for D2DR bottom docked position [30].

3.6. Root-Mean-Square Deviation of Atom Distances

Unlike a typical RMSD analysis, the root-mean-square of the differences in atom-pair distance measurements does not need least-square fitting of the structures to the reference ones. [30].

In agreement with high RMSF profiles observed for the FLB ligand, a maximum atom-pair average distance of 0.15 nm was determined for the same ligand docked on both D2DR positions. When compared to the ligands docked at the top of D2DR, the average atom-pair distances for ligands located at the bottom of the receptor slightly increased (Figure 3.5). For instance, the average values of the RACL ligand increased from 0.094 nm (docked at D2DR's top part) to 0.116 nm (docked at D2DR's bottom part) [30].

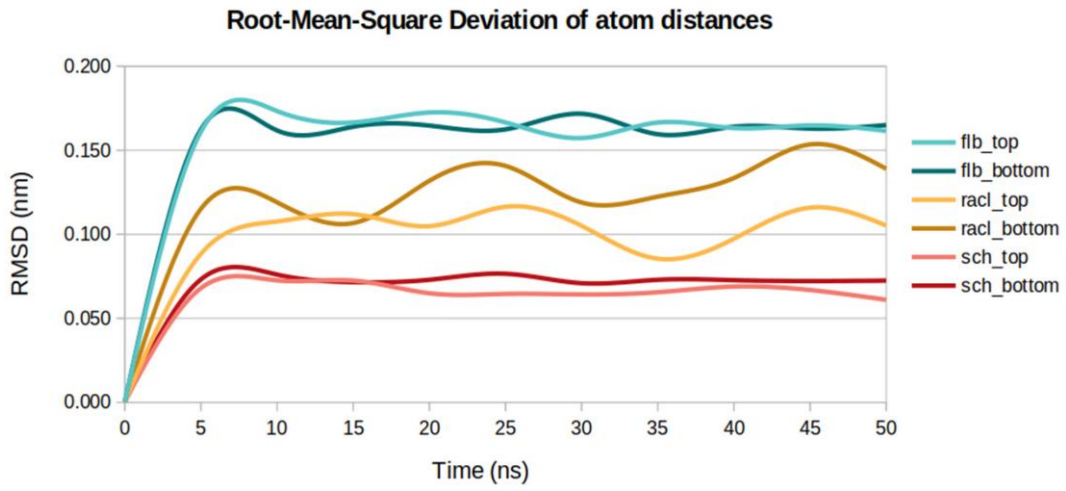

Figure 3.5. *- Atom-pair distances for the three ligands docked at the top and bottom parts of D2DR [30].*

The SCH ligand show the smallest atom-pair distances among all ligands for both D2DR docked positions, with an average atom distance of 0.06 nm for the top part of the receptor and 0.07 nm for the bottom one. In addition, the atom-pair distances for SCH ligand are correlated

with the ligand's RMSF average value of 0.06 nm and its lower gyration profile (of 0.34 nm) for both receptor extremities.[30].

As expected, the RACL atom-pair distances are correlated to the RMSD profiles of the ligand (0.04 nm between D2DR top and bottom sites). Furthermore, when the top docked position was compared to the bottom one, a difference of 0.03 nm was noted. The same value was observed for RMSF measurements (0.12 nm for RACL docked at D2DR top pocket and 0.15 nm for RACL located at D2DR's bottom pocket) [30].

3.7. Total Interaction Energies

The total interaction energies were determined using two components: Coulombic short-range interactions and Lennard–Jones potentials. The interaction energies for the D2DR–RACL ligand docked at D2DR's top position had the highest average absolute value of 150.04 kJ/mol. The SCH ligand showed a similar total energy of 147.59 kJ/mol (Tables 3.3 and 3.4). Surprisingly, the SCH ligand had the highest interaction energy (of 164.22 kJ/mol) among all ligands docked at D2DR's bottom part. Moreover, an interesting energetic behavior was seen for the SCH and RACL docked ligands, where their energy patterns were very similar considering their different docked positions. Specifically, a total interaction energy of 147 kJ/mol was observed for the SCH ligand docked at D2DR's top position, and the same interaction energy was seen for the RACL ligand docked at D2DR's bottom position [30].

Table 3.3. *- Total interaction energies (calculated as the sum between Coulombic and Lennard-Jones interactions) for the three ligands docked at D2DR's top position [30].*

FLB		RACL		SCH	
Coul-SR (kJ/mol)	L-J-SR (kJ/mol)	Coul-SR (kJ/mol)	L-J-SR (kJ/mol)	Coul-SR (kJ/mol)	L-J-SR (kJ/mol)
−11.09	−124.40	−22.64	−127.40	−30.33	−117.26
Total Energy: −135.50 kJ/mol		Total Energy: −150.04 kJ/mol		Total Energy: −147.59 kJ/mol	

Table 3.4. *- Total interaction energies (calculated as the sum between Coulombic and Lennard-Jones interactions) for the three ligands docked at D2DR's bottom position [30].*

FLB		RACL		SCH	
Coul-SR (kJ/mol)	**L-J-SR (kJ/mol)**	**Coul-SR (kJ/mol)**	**L-J-SR (kJ/mol)**	**Coul-SR (kJ/mol)**	**L-J-SR (kJ/mol)**
−10.01	−96.12	−24.84	−122.94	−26.15	−138.07
Total Energy: −106.13 kJ/mol		Total Energy: −147.78 kJ/mol		Total Energy: −164.22 kJ/mol	

Lower interaction energies of 135.50 kJ/mol and 106.13 kJ/mol were observed for the FLB molecule docked in both D2DR's pockets. Overall, the ligands situated at the top part of D2DR presented higher energy patterns compared to the ligands docked at the bottom part of the receptor. In contrast, the SCH ligand bound at the bottom part of D2DR had the highest interaction energy value [30].

4. Conclusions and Perspectives

Our docking results predicted that ^{11}C-labeled FLB and RACL ligands exhibit increased binding affinities at the receptor's top. At this level, the absolute interaction energies of RACL and FLB ligands were 147.78 and 106.13 kJ/mol, respectively. SCH ligand presented the highest absolute interaction energy for the bottom site of the receptor, while RACL ligand exhibited the strongest interaction pattern when docked at the top part of D2DR. In addition, the RACL ligand in D2DR's top position and the FLB ligand docked at the opposite D2DR pocket had the highest docking scores. While the FLB ligand has a predisposition to leave the receptor's bottom pocket, the SCH and RACL ligands show higher binding affinities, while remaining inside both D2DR docked pockets. As a result, a maximum solvent exposure area of 5.63 nm2 was observed/obtained for the FLB ligand docked at the lower part of D2DR.

The Rg profiles for all ligands indicated a constant gyration behavior, particularly for the FLB and RACL ligands that showed comparable gyration average values for both D2DR docked positions. The SCH ligand had a slight decrease in the average Rg value when the two opposing docking pockets were examined. The FLB ligand situated at the top part of the receptor was correlated with the highest atomic RMSD values among all complexes. In addition, this ligand also presented the largest interatomic distances for both of its docking positions.

Consequently, based on our findings, the RACL ligand docked at the top pocket of D2DR and the SCH ligand considered at the bottom part of the receptor are the most efficient ligands in terms of interaction strength within the receptor–ligand complexes studied and discussed in the present thesis.

Perspectives consist of further MD studies with extensive production time and free energy calculations. The same set of ligands will be docked in the top pocket of the receptor, with the D2DR structure embedded in a DOPC/phospholipid bilayer membrane.

The following research focuses on DOPC [31] membrane, which is a phosphatidylcholine (PC) belonging to the class of phospholipids that include choline as a headgroup. They are an essential component of biological membranes and may be extracted mechanically or chemically

from a number of widely accessible sources, such as egg yolk or soybeans, using hexane. Phosphatidylcholines are present in all plant and animal cells, but not in the membranes of most bacteria, including E. coli. [32] and it is manufactured commercially.

Figure 4.1 is an example of D2DR-LIG-DOPC system that we have been able to model.

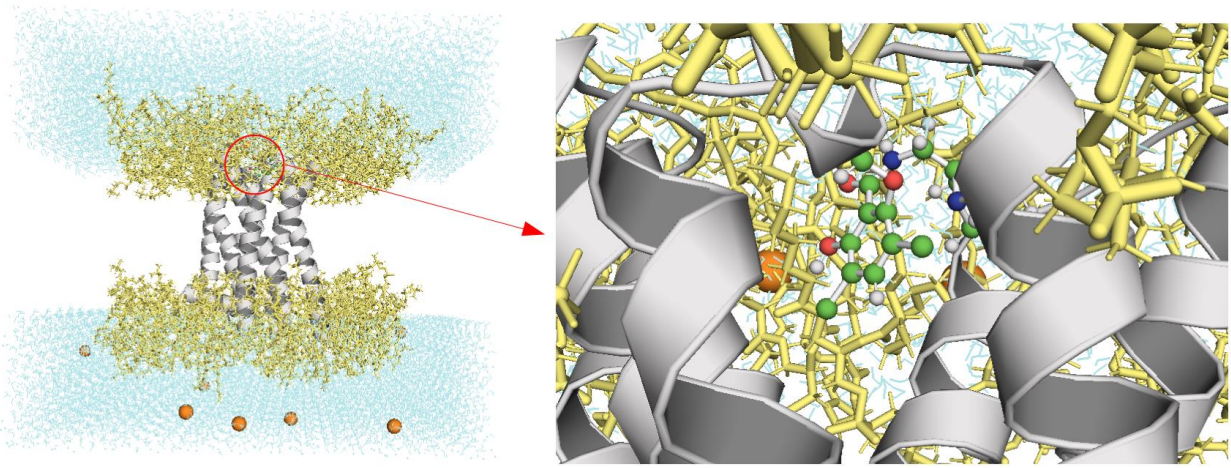

Figure 4.1. *– RACL inside the top pocket of the D2DR-LIG-DOPC system*

Similar to the herein presented study [30], the purpose of our future research is to determine the strength of the interactions between the same set of ligands with the D2 dopamine receptor.

The workflow of the D2DR-LIG-DOPC system simulation is fairly similar to that of the D2DR-LIG system. The difference between these studies is, the presence of the DOPC membrane. This addition requires changes in the methodology. For instance, due to the fact that the D2DR is being embedded in the membrane, the only docking site that is going to be analyzed is the top part of the receptor. Furthermore, we expect higher values of the initial potential energy of the system that will require additional steps (we need to minimize the system's energy in more steps). Nevertheless, the addition of the membrane requires a larger simulation box and more computational power. Last but not least, with the addition of the DOPC membrane we hope to achieve an even more accurate simulation of the physiological receptor-ligand interacting system.

Acknowledgments

This research was conducted with the use of computational resources provided by Babeș-Bolyai University, Faculty of Physics, Cluj-Napoca, Romania. My thanks to Dr. Sanda Moldovean-Cioroianu (Biomolecular Physics, Faculty of Physics, Babeș-Bolyai University, Cluj-Napoca, Romania) for her constant reviews on this paper and for sharing her knowledge in MD simulations. My thanks to Prof. Dr. Vasile Chiș (Babeș-Bolyai University, Faculty of Physics, Cluj-Napoca, Romania) for supervising our work.

References

1. Sagui, C., Darden, T. A. *Molecular dynamics simulations of biomolecules: long-range electrostatic effects.* Annu Rev Biophysics Biomolecular Struct., **28**, 155–179, 1999, DOI: 10.1146/annurev.biophys.28.1.155.

2. Parrinello M. *From silicon to RNA: the coming of age of ab initio molecular dynamics.* Solid State Commun., **102**, 107–120, 1997, DOI: 10.1016/S0038-1098(96)00723-5.

3. Köhler, C., Hall, H., Ogren, S. O., Gawell, L. *Specific in vitro and in vivo binding of 3H-raclopride. A potent substituted benzamide drug with high affinity for dopamine D-2 receptors in the rat brain.* Biochemical pharmacology., **34**, 2251–2259, 1985, DOI: 10.1016/0006-2952(85)90778-6.

4. Antonini, A., Leenders, K. L., Spiegel, R., et al. *Striatal glucose metabolism and dopamine D2 receptor binding in asymptomatic gene carriers and patients with Huntington's disease.* Brain., **119**, 2085–2095, 1996, DOI: 10.1093/brain/119.6.2085.

5. Farde, L., Gustavsson, J. P., & Jönsson, E. *D2 dopamine receptors and personality traits*. Nature, **385**, 590, 1997, DOI: 10.1038/385590a0.

6. Derlet, R. W., Albertson, T. E., Rice, P. *The effect of SCH 23390 against toxic doses of cocaine, d-amphetamine and methamphetamine*. Life sciences, **47**, 821–827, 1990, DOI: 10.1016/0024-3205(90)90555-6.

7. Högberg, T., de Paulis, T., Johansson, L., Kumar, Y., Hall, H., Ogren, S. O. *Potential antipsychotic agents. 7. Synthesis and antidopaminergic properties of the atypical highly potent (S)-5-bromo-2,3-dimethoxy-N-[(1-ethyl-2-pyrrolidinyl)methyl]benzamide and related compounds. A comparative study.* J med chem., **33**, 2305–2309, 1990, DOI: 10.1021/jm00170a040.

8. Högberg, T., Ström, P., Hall, H., Ögren, S. O., *Potential antipsychotic agents. Part 8†. Antidopaminergic properties of a potent series of 5-substituted (−)-(S)-N -[(1-ethylpyrrolidin-2-yl)methyl]-2,3-dimethoxybcnzaimides. Synthesis via common lithio intermediates.* Helvetica Chimica Acta, **73**, 417-425, 1990, DOI: 10.1002/hlca.19900730221.

9. Hall, H., Högberg, T., Halldin, C., Bengtsson, S., Wedel, I. *Synthesis and binding properties of the fluorinated substituted benzamide [3H]NCQ 115, a new selective dopamine D2 receptor ligand.* Eur J Pharmacol., **201**, 1–10, 1991, DOI: 10.1016/0014-2999(91)90315-h.

10. Halldin, C., Farde, L., Högberg, T., Mohell, N., Hall, H., Suhara, T., Karlsson, P., Nakashima, Y., & Swahn, C. G. *Carbon-11-FLB 457: a radioligand for extrastriatal D2 dopamine receptors*. J Nucl Med., **36**, 1275–1281, 1995, PMID: 7790956.

11. Kalani, M. Y., Vaidehi, N., Hall, S. E., Trabanino, R. J., Freddolino, P. L., Kalani, M. A., Floriano, W. B., Kam, V. W., Goddard, W. A., 3rd *The predicted 3D structure of the human D2 dopamine receptor and the binding site and binding affinities for agonists and antagonists.* Proc Natl Acad Sci U S A., **101**, 3815–3820, 2004, DOI: 10.1073/pnas.0400100101.

12. Wang, S., Che, T., Levit, A., Shoichet, B. K., Wacker, D., Roth, B. L. *Structure of the D2 dopamine receptor bound to the atypical antipsychotic drug risperidone.* Nature, **555**, 269–273, 2018, DOI: 10.1038/nature25758.

13. Trabanino, R. J., Hall, S. E., Vaidehi, N., Floriano, W. B., Kam, V. W., Goddard, W. A., 3rd. *First principles predictions of the structure and function of g-protein-coupled receptors: validation for bovine rhodopsin.* Biophys J, **86**, 1904–1921, 2004, DOI: 10.1016/S0006-3495(04)74256-3.

14. Rigsby, R. E., Parker, A. B. *Using the PyMOL application to reinforce visual understanding of protein structure.* Biochem Mol Biol Educ, **44**, 433–437, 2016, DOI: 10.1002/bmb.20966.

15. **Crișan, G., Moldovean-Cioroianu, N. S., Timaru, D. G., Andrieș, G., Căinap, C., Chiș, V. *Radiopharmaceuticals for PET and SPECT Imaging: A Literature Review over the Last Decade*. Int J Mol Sci., 23, 5023, 2022, DOI: 10.3390/ijms23095023.**

16. Schlick, T. *Pursuing Laplace's Vision on Modern Computers*. In: Mesirov, J.P., Schulten, K., Sumners, D.W. (eds) Mathematical Approaches to Biomolecular Structure and Dynamics. The IMA Volumes in Mathematics and its Applications, **82**, 219-247, 1996, DOI: 10.1007/978-1-4612-4066-2_13.

17. Alder, B. J., Wainwright, T. E. *Studies in Molecular Dynamics. I. Generated Method.* J Chem Phys., **31**, 459, 1959, DOI: 10.1063/1.1730376.

18. The GROMACS development team, *GROMACS Documentation 2020.*

19. Vanommeslaeghe, K., Hatcher, E., Acharya, C., Kundu, S., Zhong, S., Shim, J., Darian, E., Guvench, O., Lopes, P., Vorobyov, I., Mackerell, A. D., Jr. *CHARMM general force field: A force field for drug-like molecules compatible with the CHARMM all-atom additive biological force fields.* J Comp Chem., **31**, 671–690, 2010, DOI: 10.1002/jcc.21367.

20. M. A. Gonzales. *Force fields and molecular dynamics simulations*, JDN, **12**, 169-200, 2011, DOI: 10.1051/sfn/201112009.

21. Rapaport, D. C. *The Art of Molecular Dynamics Simulation (2nd ed.)*. Cambridge University Press. Bar-Ilan University, Israel, 2004.

22. Pettersen, E.F., Goddard, T.D., Huang, C.C., Couch, G.S., Greenblatt, D.M., Meng, E.C., Ferrin, T.E. *UCSF Chimera—A visualization system for exploratory research and analysis.* J. Comput. Chem., **25**, 1605–1612, 2004, DOI: 10.1002/jcc.20084.

23. Van Der Spoel, D., Lindahl, E., Hess, B., Groenhof, G., Mark, A.E., Berendsen, H.J. *GROMACS: Fast, flexible, and free.* J. Comput. Chem., **26**, 1701–1718, 2005, DOI: 10.1002/jcc.20291.

24. Lengauer, T., Rarey, M. *Computational methods for biomolecular docking.* Curr. Opin. Struct. Biol., **6**, 402–406, 1996, DOI: 10.1016/s0959-440x(96)80061-3.

25. Kitchen, D.B., Decornez, H., Furr, J.R., Bajorath, J. *Docking and scoring in virtual screening for drug discovery: Methods and applications.* Nat. Rev. Drug Discov., **3**, 935–949, 2004, DOI: 10.1038/nrd1549.

26. Grosdidier, A., Zoete, V., Michielin, O. *SwissDock, a protein-small molecule docking web service based on EADock DSS.* Nucleic Acids Res., **39**, W270–W277, 2011, DOI: 10.1093/nar/gkr366.

27. Jorgensen, W.L., Chandrasekhar, J., Madura, J.D., Impey, R.W., Klein, M.L. *Comparison of simple potential functions for simulating liquid water.* J. Chem. Phys., **79**, 926–935, 1983, DOI: 10.1063/1.445869.

28. Berendsen, H.J.C., Postma, J.P.M., van Gunsteren, W.F., DiNola, A., Haak, J.R. *Molecular-Dynamics with Coupling to an External Bath.* J. Chem. Phys., **81**, 3684–3690, 1984, 10.1063/1.448118.

29. Hess, B., Kutzner, C., van der Spoel, D., Lindahl, E. *GROMACS 4: Algorithms for Highly Efficient, Load-Balanced, and Scalable Molecular Simulation.* J. Chem. Theory Comput., **4**, 435–447, 2008, DOI: 10.1021/ct700301q.

30. **Moldovean, S. N., Timaru, D. G., Chiş, V. *All-Atom Molecular Dynamics Investigations on the Interactions between D2 Subunit Dopamine Receptors and Three ^{11}C-Labeled Radiopharmaceutical Ligands.* International journal of molecular sciences, 23, 2005, 2022. DOI: 10.3390/ijms23042005.**

31. Ulrich, A. S., Sami, M., Watts, A. *Hydration of DOPC bilayers by differential scanning calorimetry*. Biochimica et Biophysica Acta (BBA) - Biomembranes, **1191**, 225–230, 1994, DOI: 10.1016/0005-2736(94)90253-4.

32. Suzanne Jackowski, John E. Cronan, Charles O. Rock. *Chapter 2 Lipid metabolism in procrayotes.* New Comprehensive Biochemistry. **20**, 43-85, 1991. DOI: 10.1016/S0167-7306(08)60330-0.

Anexa 2

DECLARAȚIE PE PROPRIE RĂSPUNDERE

Subsemnata, DIANA-GABRIELA TIMARU, declar că Lucrarea de licență/diplomă/disertație pe care o voi prezenta în cadrul examenului de finalizare a studiilor la Facultatea de Fizică, din cadrul Universității Babeș-Bolyai, în sesiunea IUNIE 2022 , sub îndrumarea Prof. Dr. VASILE CHIȘ, reprezintă o operă personală. Menționez că nu am plagiat o altă lucrare publicată, prezentată public sau un fișier postat pe Internet. Pentru realizarea lucrării am folosit exclusiv bibliografia prezentată și nu am ascuns nici o altă sursă bibliografică sau fișier electronic pe care să le fi folosit la redactarea lucrării.

Prezenta declarație este parte a lucrării și se anexează la aceasta.

Data,

21.06.2022

Nume,

Diana -Gabriela TIMARU

Semnătură